Semicond. Sci. Technol. 9 (1994) 1316–1323. Printed in the UK

One-dimensional Monte Carlo analysis of electron transport in submicrometre silicon structures

M J Martín, T González, D Pardo and J E Velázquez

Departamento de Física Aplicada, Facultad de Ciencias, Universidad de Salamanca, 37008 Salamanca, Spain

Received 20 October 1993, in final form 28 February 1994, accepted for publication 17 March 1994

Abstract. By coupling an ensemble Monte Carlo simulator with a one-dimensional Poisson solver, we analyse anisotropic electron transport in homogeneous Si structures and submicrometre n^+nn^+ diodes. The model employed for the conduction band in the simulation approximates the real band by means of non-parabolic ellipsoidal X and L valleys. An energy limit for the energy that the electron can reach in the X valleys has been established. Firstly, in order to check the validity of the band model over a wide range of electric fields a study of anisotropic electron transport in bulk Si has been performed. On the basis of bulk Si results, the electron transport properties in both structures have been thoroughly explained by the analysis of the static characteristics. Special attention is paid to the origin of the anisotropic effects, which are explained in terms of the different occupation of the X valleys. The L valleys are found to have an influence for the highest fields.

1. Introduction

The study of electron transport in semiconductors at very high electric fields has reached an important stage in the last few years. The reduction of the MOSFET gate length causes a degradation of device electric behaviour as a result of the elevated fields reached in the channel.

One of the phenomena that appears at very high electric fields is the impact ionization effect, which limits the normal operation of some devices but is a basic phenomenon in the behaviour of other devices (for example avalanche photodetectors). Moreover, there are devices based on extremely energetic electrons which bear elevated electric fields in some regions (for example hot-electron transistors). These facts justify the inclusion of a suitable electron and hole transport description in device simulators for very high electric field conditions. In the present work we have limited our attention to the case of electron transport. Therefore our unipolar model can be applied up to the bias voltage at which the impact ionization processes begin.

Non-equilibrium transport effects in small semiconductor devices have generated great interest in methods that, by solving the Boltzmann transport equation (BTE), deal with the problem of carrier transport at a microscopic level [1, 2]. The drift-diffusion model, because it assumes a thermal equilibrium of mean carrier energy, is not accurate enough for submicrometre device modelling [3, 4]. The approaches based on the hydrodynamic and energy-transport/balance models [5] cannot give a self-consistent description of the carrier transport. Nowadays the microscopic transport model based on the Monte Carlo (MC) method to solve the BTE seems to be the most adequate for the complete study of submicrometre and nanometre electronic devices [1, 6–9]. This method is used as a reference to evaluate the accuracy of the other simplified approaches, which need to extract certain transport coefficients from MC simulations and are only more efficient from the point of view of CPU time.

In this paper we deal with electron transport in Si, in which a very important factor is the model used to represent the band structure. The lower set of minima of the first conduction band described by analytical formulae do not describe adequately the physical properties of high-energy electrons. A full band structure obtained from empirical pseudopotential calculation is the most accurate model [10–13] to perform the MC simulation of bulk Si. However, this model aggravates the computational time problem for the study of dynamic behaviour (analysis of noise, equivalent circuits etc) in small solid state structures.

The purpose of this paper is to analyse electron transport in homogeneous and n^+nn^+ Si structures by means of a simple anisotropic model for the band structure. This model, which includes ellipsoidal X and L valleys, is able to describe the carrier transport in this

0268-1242/94/071316+08$19.50

material subject to an extensive range of electric fields, including the effects of anisotropy.

The MC method has already been applied to the study of the n^+nn^+ diode as a simple approach to FETs, extensively in GaAs [14, 15] and also in the case of Si, but with an isotropic band model including only the set of X valleys [16–18].

The organization of this paper is as follows. In section 2 we present the anisotropic conduction model employed in the simulation, together with some results obtained in bulk silicon (drift velocity and valley occupation). Next, in section 3, we present the MC procedure for device simulation and the physical model used for the different simulated structures. In section 4, we report the detailed results related to the dependence of the static characteristics of the homogeneous and n^+nn^+ structures on the field direction ($\langle 100 \rangle$ and $\langle 111 \rangle$). Finally we summarize the main conclusions.

2. Electron transport in bulk Si

Before applying our transport model to the simulation of Si devices, and in order to check its validity, we have carried out the study of electron transport in bulk Si. Such a study allows us to fit the values of certain parameters in our model with the aim of adequately describing low (velocity–field relation) and high electric field transport (impact ionization coefficient–electric field relation).

In this section we describe the conduction band (section 2.1). Later we report the most important results from the bulk Si MC simultation in section 2.2.

2.1. Conduction band model

Our Si conduction band model approximates the first conduction band by means of two kinds of valleys: X and L. Both valleys are considered to be non-parabolic ellipsoidal in the same way as in [19]. The equivalent X valleys have a limit to the energy that the electron can reach in them, as takes place in the real band. In the L valleys no energy limit has been considered.

The electron energy limit criterion has been taken into account successfully in previous works for different semiconductor materials [20, 21]. The effect of the X-valley energy limit on the carrier movement can be excessively sharp if the carrier free flight is truncated when the electron reaches the energy limit. In order to do it softly, we establish two energy limits. The value we have considered for the first one is 2.15 eV, equal for the six equivalent valleys. The second limit we have established is 2.65 eV. Both values are measured from the bottom of the conduction band.

Figure 1 shows the band structure model employed in our simulation, together with the full conduction band calculated by [22] through a pseudopotential method. The analytical model reproduces properly the real first band structure. It can be observed that the first limit chosen for the X valley is similar to the

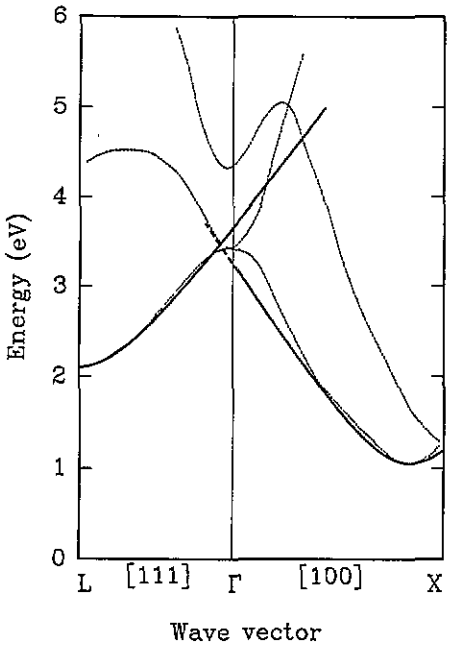

Figure 1. First, second and third conduction bands of the real band structure from [22] (dotted curve) and valley approximation of the real band structure of the present model (full curve; the broken curve corresponds to the energy interval between the two energy limits).

energy for which the change in the sign of the real conduction band curvature occurs. Both first and second limits have been chosen within a range by fitting the whole set of experimental data on the impact ionization coefficient [23–26]. Morover, we have taken into account the adjustment of the drift velocity–electric field characteristic in the considered range of electric fields.

We include these two limits in the MC simulation as follows: when a carrier is in an X valley with a kinetic energy above the first energy value, only those scattering probabilities corresponding to the non-equivalent intervalley mechanisms (X–L) are different from zero, which means that the carrier must leave the X valley at the end of the free flight if its energy is above this first energy limit. At the same time, if the carrier is one of the L valleys and its total energy is above the first limit, the scattering rates corresponding to the L–X intervalley mechanisms are equal to zero; therefore the electron must remain in an L valley.

The second energy limit is established so that no carrier in the X valleys can finish a free flight with an energy value above this limit. Should this occur, the free flight is rejected, and a random number is selected again in order to determine its duration until the final energy of the flight does not exceed this second limit.

In this way, the X-valley energy limit is not a hard limit, since the carrier does not pass to the upper valley just when it attains the first energy value, but when the carrier ends the free flight in which this energy limit is surpassed.

2.2. Bulk Si simulation

The MC method employed here has been extensively described by other authors [27]. The physical parameters

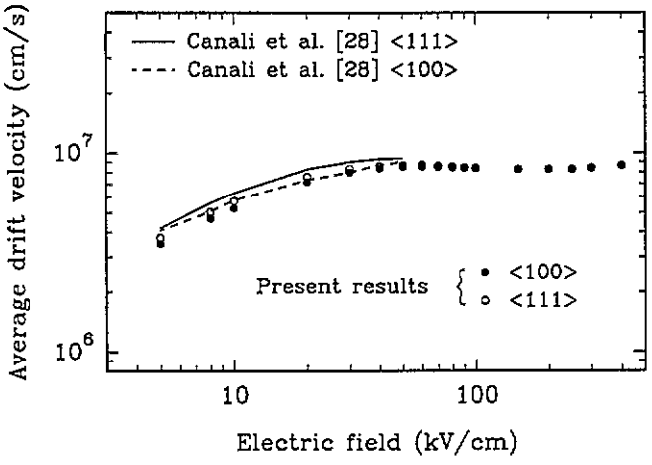

Figure 2. Average drift velocity as a function of the electric field between 5 and 500 kV cm^{-1} along the ⟨100⟩ and ⟨111⟩ crystallographic directions. The experimental results are taken from [28]. The simulation results were obtained with a density of ionized impurities of $N_D = 10^{13}$ cm^{-3}.

and the scattering mechanisms considered are the same as used in [19].

We study the trajectory of an electron in both real and k-space in an n-type homogeneous semiconductor subject to the action of a constant electric field. The simulation was performed at 300 K, for an electric field applied in the ⟨100⟩ and ⟨111⟩ directions.

The electron average drift velocity is shown in figure 2 as a function of the applied field in both directions for the range 5–500 kV cm^{-1}. The experimental results are taken from [28]. A slight anisotropy is observed, and a slight negative differential mobility appears around 100–150 kV cm^{-1} due to the onset of X–L intervalley mechanisms. The negative differential mobility has also been found by Sano *et al* [29].

Figure 3 shows the fraction of time that the electron remains in each valley as a function of the electric field in the ⟨100⟩ and ⟨111⟩ directions. The difference in the occupation of the X valleys between the two directions of the applied voltage is the origin of the anisotropy observed in the average drift velocity (figure 2). When the voltage is applied in the ⟨111⟩ direction, the parallel and perpendicular X valleys are equally populated, and the same occurs in the L valleys.

As we explained before, we have introduced an energy limit in the X valleys. As a consequence of that, different occupancy of the different valleys between the present results and those reported in [19] appears at high electric fields, as can be observed in the figures. Understanding of the effect of the large L-valley occupation is essential if we are to understand the results at high electric fields in both material and devices.

There is no effect of anisotropy in the occupancy of the L valleys. The presence of electrons in these valleys begins to be appreciable for electric fields above 70 kV cm^{-1}. As the field increases, the total occupation of the L valleys becomes more important, reaching a value near 40% for 500 kV cm^{-1}.

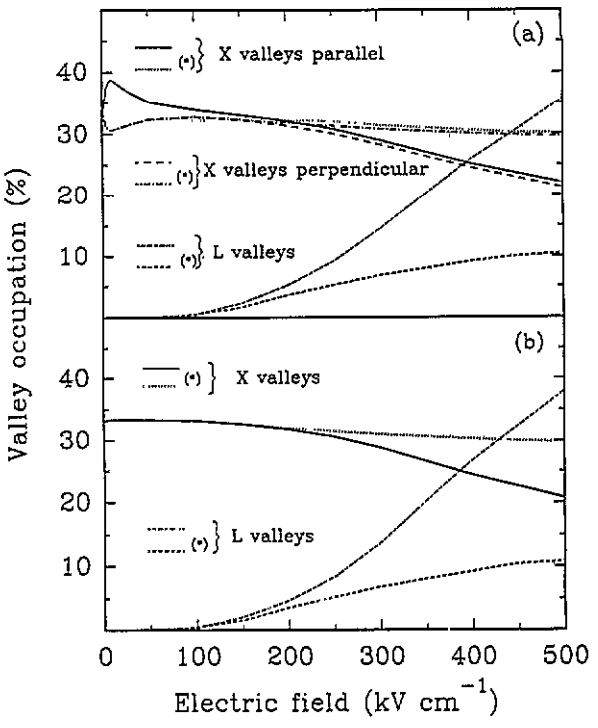

Figure 3. Fraction of time that the electron remains in the parallel and perpendicular X valleys in the L valleys as a function of the electric field between 0 and 500 kV cm^{-1}. (*a*) Electric field applied in the ⟨100⟩ direction. (*b*) Electric field applied in the ⟨111⟩ direction. (*) Previous model results [19]. The results for perpendicular X valleys are the same, so we only report the results of one of them. The line of the L valleys corresponds to the total occupation of the four L valleys.

3. Monte Carlo device simulation

The transport in small devices differs from bulk transport in significant aspects: the structures are spatially limited and the presence of inhomogeneities leads to non-uniform field profiles. Thus, it is very important to take into account the time evolution of the electric field self-consistently with the charge motion, by periodically solving the Poisson equation with appropriate boundary conditions.

3.1. One-dimensional Monte Carlo simulator

The simulation consists of the study of the real and k-space dynamics of the charge carriers in a well defined potential distribution. Degeneracy effects and electron–electron scattering are not included in the model, since for the doping profiles considered in the devices these effects are negligible.

The calculation of the physical quantities of interest is carried out by coupling self-consistently a one-dimensional Poisson solver (PS) with an ensemble MC simulator, three-dimensional in k-space and one-dimensional in real space. The MC simulation follows the standard scheme [6]. The structures are divided into equal cells of 10^{-6} cm each, a width that is smaller than the Debye length corresponding to the highest doping considered. The field is updated each 10 fs, which fulfils the two stability criteria related to the plasma

frequency (for X and L valleys) [30] and to the dielectric relaxation time [31]. The cloud-in-cell algorithm is employed to assign the particle charge to the mesh nodes. The Poisson equation is solved by means of a very simple Gaussian elimination method for the three-diagonal systems [32].

The carriers are initially placed into the device with the wavevector randomly selected according to a Maxwell–Boltzmann distribution at the lattice temperature, and their positions are determined according to the doping profile, so that charge neutrality is achieved in the device at the beginning of the simulation. The voltage is applied, and once the steady state is reached (30 ps), statistics of all physical quantities (velocity, density etc) are collected.

In order to obtain an accurate solution of the electric field, and to reduce the CPU time required for the simulations, we consider it appropriate to initially simulate a number of particles around 12 000 in the n^+nn^+ structure and 20 000 in the homogeneous one. Each simulated particle is equivalent to 5×10^8 electrons/cm^2 [16].

3.2. Simulated structures

We have analysed two Si structures at room temperature: the first is a 0.3 μm (n^+)–0.4 μm (n)–0.3 μm (n^+) diode with two abrupt homojunctions along the simulated direction, and the second is an n-type homogeneous structure, 1 μm long. In each case the total length of the device is the same.

The doping concentration of the homogeneous structure is 10^{17} cm^{-3} and the doping of the n^+ and n regions in the n^+nn^+ structure is 10^{17} and 10^{15} cm^{-3} respectively.

The Si band model we employ is the one described in section 2. The anisotropy that appears in bulk silicon must have an effect on the performance of the devices. In order to analyse that effect in both structures, the simulation has been carried out for the electric fields in the ⟨100⟩ and ⟨111⟩ directions.

3.3. Boundary conditions

The model employed for simulating the electrodes is called the ohmic boundary condition [30]. Both electrodes are modelled as ideal ohmic contacts: the free carrier concentration of a small region (one grid cell) close to each contact should remain constant and equal to the doping density, and the carrier mean energy must be the thermal energy in those regions. During the simulation, at the end of each time-step the concentration in both contact cells is tested and, if necessary, carriers are injected into the electrodes at thermal equilibrium, with energy and momentum determined according to the Maxwell–Boltzmann distribution at the lattice temperature.

We apply a constant voltage between the contacts, and calculate the static macroscopic magnitudes, free-carrier density, velocity and current density, as a function of the applied voltage (J–V).

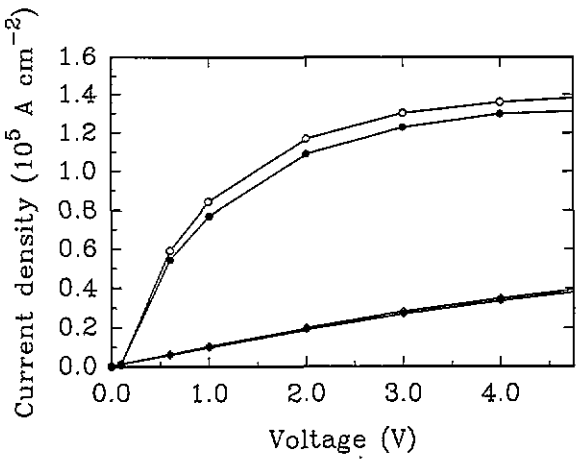

Figure 4. Current density as a function of the applied voltage in the n^+nn^+ (diamonds) and the homogeneous (circles) structures as a function of the applied voltage in the ⟨100⟩ direction (full symbols) and the ⟨111⟩ direction (open symbols). The length of the devices is equal to 1.0 μm.

3.4. Results

In this section we report the static results of the simulations for homogeneous and n^+nn^+ structures oriented along the ⟨100⟩ and ⟨111⟩ crystallographic directions when the applied voltage varies between 0 and 4 V.

To highlight the anisotropy effect we show the differences of the results for the mean drift velocity between the two directions of the electric field as a function of the position inside the device. We only present the results of free-carrier density, energy, electric field and potential across the device for the bias applied in the ⟨100⟩ direction, because the anisotropy effect at such magnitudes is not significant.

Figure 4 shows the current density (J)–bias voltage (V) chracteristics of the homogeneous and n^+nn^+ structures described in section 3.2. We can observe two well defined regions: for low voltage the current density increases linearly with V; for higher applied bias a current saturation region appears. The change from the linear to the saturation region is more pronounced for the homogeneous structure, in which the current situation occurs at a lower voltage than in the n^+nn^+ structure. Notice that the current density is greater when the voltage is applied in the ⟨111⟩ direction, in agreement with the bulk Si drift velocity behaviour.

In figure 5 we report the number of particles that remain inside the devices versus V. This number stays nearly constant in the n^+nn^+ structure in the considered range regardless of the bias voltage direction. For voltages between 0 and 3 V in the homogeneous structure the particle number remains practically constant in the device. For high voltages a slight increment in the particle number appears in the homogeneous device, which is more pronounced when the voltage is applied in the ⟨111⟩ direction.

To interpret these results we must first refer to the static characteristics of the homogeneous structure. Figures 6(a)–(d) show the free-carrier density,

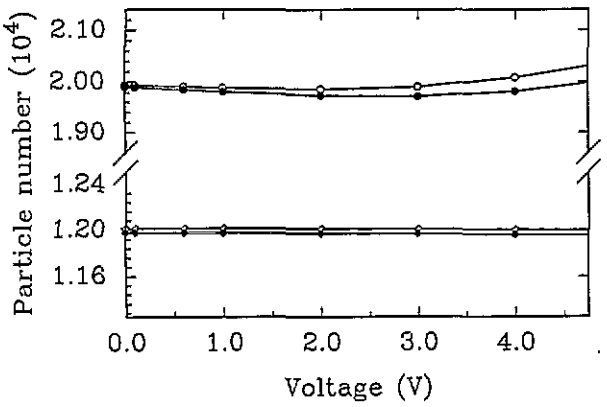

Figure 5. Number of simulated particles inside the n^+nn^+ (diamonds) and the homogeneous (circles) structures as a function of applied voltage in the ⟨100⟩ (full symbols) and ⟨111⟩ (open symbols) directions.

energy, potential and electric field profiles along the homogeneous structure for different biases.

It can be observed that the free-carrier concentration (figure 6(*a*)) has a uniform value along the device. As we have remarked before, for bias voltage below 3 V the number of particles inside the device is practically constant. Therefore, the free-carrier concentration is equal to the doping profile. This carrier density behaviour makes the potential increase linearly as a function of the position in the device, that is, the bias voltage uniformly drops along the structure. So the electric field (figure 6(*d*)) stays constant in the device and increases with the applied voltage. For bias voltage above 3 V the increment of the particle number is reflected in the increase of the free-carrier concentration, leading to the linear dependence of the electric field on the position.

The effect of the carrier injection at the ohmic contacts affects slightly the static characteristics in the vicinity of the contacts. The global influence of such an effect on the current density results is negligible.

In the homogeneous structure, we find that the drift velocity has no spatial dependence in the device (except near the contacts). Thus, we do not report the profile of the drift velocity along the structure but its dependence on the applied voltage in both crystallographic directions (figure 7). It can be observed that, after a linear region, another saturation region appears, whose origin is the same as in bulk Si [19]. This quick saturation in the velocity is the main reason for the current saturation in the homogeneous structure. The maximum of the anisotropy effect in the velocity occurs when the applied voltage is equal to 1 V. This agrees with the result obtained for that magnitude in bulk Si for a field of $10\,kV\,cm^{-1}$ [19].

However, the behaviour of the current anisotropy is different from that of the velocity, and does not decrease at increasing voltages, due to the different evolution with the applied voltage of the particle number in the two directions.

In the homogeneous structure, for voltages below 3 V, the time that the electron remains in each valley

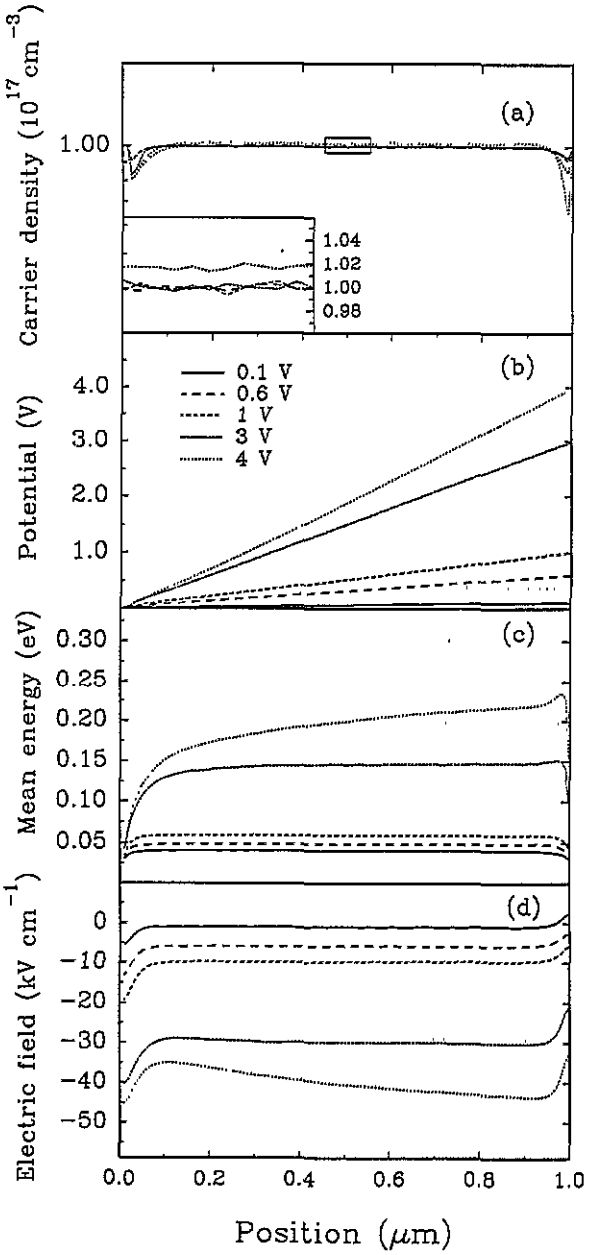

Figure 6. Profiles of free-carrier density (*a*), potential (*b*), energy (*c*) and electric field (*d*) in the homogeneous structure as a function of the position into the device for the indicated biases. The key given in (*b*) is for all four parts.

does not show a spatial dependence and its behaviour with the electric field is the same as in bulk Si (figure 3). When we apply a voltage of 4 V, the X-valley occupation is not constant along the device as a consequence of the non-uniform electric field profile for that bias (figure 6(*d*)).

Next we discuss the results obtained for the n^+nn^+ structure. The mean values of free-carrier density, electric field, potential and energy at different bias voltages as a function of the position in the n^+nn^+ structures are shown in figures 8(*a*)–(*d*).

Since doping profile in the structure is not constant, the free-carrier density shows that the electrons diffuse from the n^+ regions into the n region when no external voltage is applied. This fact leads to the appearance of a

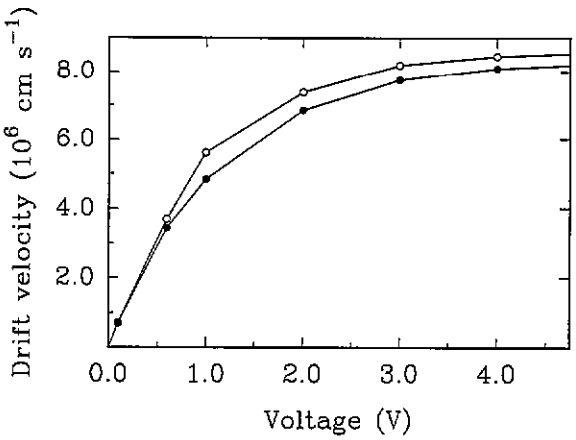

Figure 7. Average drift velocity in the homogeneous structure as a function of the voltage applied in the ⟨100⟩ direction (full circles) and ⟨111⟩ direction (open circles).

dipole of charge at the two homojunctions which induces a field opposite to the diffusion of electrons from the contact regions into the centre of the device. The peak value reached by the field is 14 kV cm^{-1}.

When a voltage is applied to the structure, the potential barrier begins to decrease in the first homojunction as the voltage increases (figure 8(*b*)), and the potential mostly drops inside the n region. As a consequence of the fall in the voltage barrier the positive value of the electric field in the first homojunction decreases. A very high negative electric field is found in the n region, which reaches a maximum in the second homojunction (figure 8(*d*)). This maximum value of the electric field in the n^+nn^+ structure is greater than the constant field appearing in the homogeneous structure for the same bias (figure 6(*d*)).

The electric field in almost all the n region is an accelerating field that provides a favourable transport condition for electrons. In this way, in the centre of the n^+nn^+ structure electrons gain energy from the field (figure 8(*c*)). For high applied bias a significant number of high-energy electrons penetrate into the cathode n^+ region. This fact means that the L valleys will be populated in the second homojunction of the n^+nn^+ structure. The cathode n^+ region is long enough for the electrons to reach thermal equilibrium at the end of the device.

The increment of the electron mass in the structure, as the energy of the carriers increases in X valleys or the transfer to the L valleys begins, is the main cause of the appearance of carrier accumulation that progressively takes place in the n region when cathode bias increases (figure 8(*a*)). As a consequence of that, a depletion region in the cathode n^+ region must appear, which follows the drop of the external bias.

Figure 9 reports the drift velocity profile along the n^+nn^+ structure at different applied voltages in both directions. It can be observed that the velocity is higher in the ⟨111⟩ direction in accordance with the bulk Si results. Moreover, the anisotropy is less pronounced than in the homogeneous structure.

When n^+nn^+ is biased, the carrier velocity increases in the n region due to the action of the high electric field

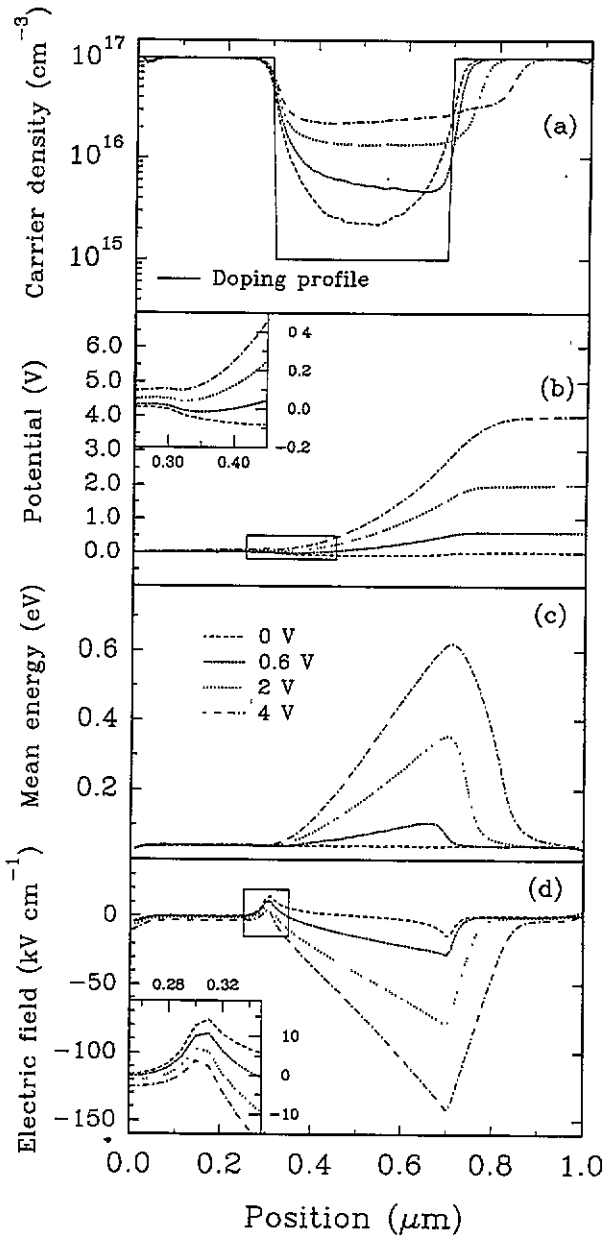

Figure 8. Profiles of free-carrier density (*a*), potential (*b*), energy (*c*) and electric field (*d*) as a function of the position in the n^+nn^+ structure for different biases. The key given in (*c*) is for all four parts.

present there. For cathode voltages higher than 2 V the field surpasses the value necessary to produce the drift velocity saturation in an important part of the n region. From that value the J–V characteristic tends to saturate slightly (figure 4). When a very high voltage of 4 V is applied, it can be observed that a decrease in the velocity near the second homojunction appears, mainly due to the electron transfer into the L valleys, which begin to be significantly occupied.

In contrast with the homogeneous structure, when the velocity saturates in the n^+nn^+ structure the carrier accumulation in the n region increases. This accumulation in the n region progressively extends towards the anode n^+ region with increasing bias, thus counteracting the effect of the velocity saturation. This is the reason why the current saturation in the n^+nn^+

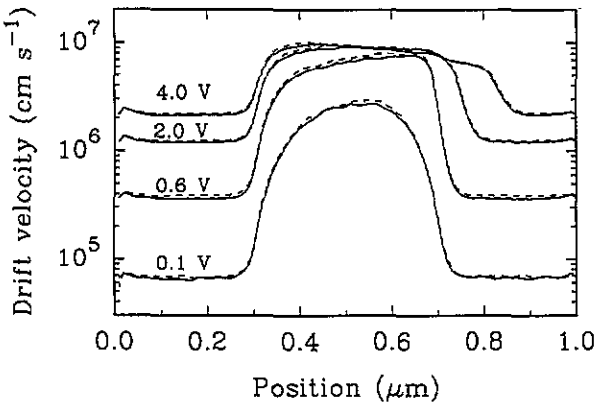

Figure 9. Drift velocity profile along the n^+nn^+ structure for the indicated applied voltages in the ⟨100⟩ direction (full curves) and ⟨111⟩ direction (broken curves).

structure is softer than in the homogeneous one.

Figures 10(*a*)–(*d*) show that the occupation of the parallel and perpendicular X valleys changes along the device due to the different values that the electric field reaches inside the n^+nn^+ structure.

The effect of non-equivalent intervalley X–L scattering is negligible for low applied voltage and most of the electrons remain in the X valleys. The maximum in the anisotropy for the X-valley occupation in bulk Si is observed around 10 kV cm^{-1}. The profile of the field in the n region of the n^+nn^+ structure changes a lot with the voltage. Thus, the spatial location of the field range for which the highest difference in the X-valley occupation occurs is displaced towards the first homojunction as the voltage increases. At the same time the anisotropy decreases in the vicinity of the second homojunction.

The bulk Si results show that the occupation of the L valleys begins to be appreciable for applied fields above 70 kV cm^{-1}. Those fields can be found near the second n^+ region when the applied voltage surpasses 2 V. These bias conditions involve the appearance of hot-electron phenomena: the drift velocity decreases, which corresponds to the slight negative differential mobility found in bulk Si due to the onset of X–L intervalley scattering (figure 2).

4. Conclusions

A microscopic study of anisotropic electron transport in unipolar Si structures has been presented. One of its special features is the straightforward approach of the real conduction band by six equivalent X valleys (with an energy limit) and four L valleys. All of them are considered as non-parabolic ellipsoids. This band model allows us to obtain a complete description of electron transport in bulk Si for a large range of electric fields. Furthermore the computer times required to get accurate results are quite acceptable, thus allowing an extension of the model towards device simulation. The anisotropic MC model described here has been implemented in an ensemble MC simulator coupled with a one-dimensional Poisson solver to study a homogeneous structure and

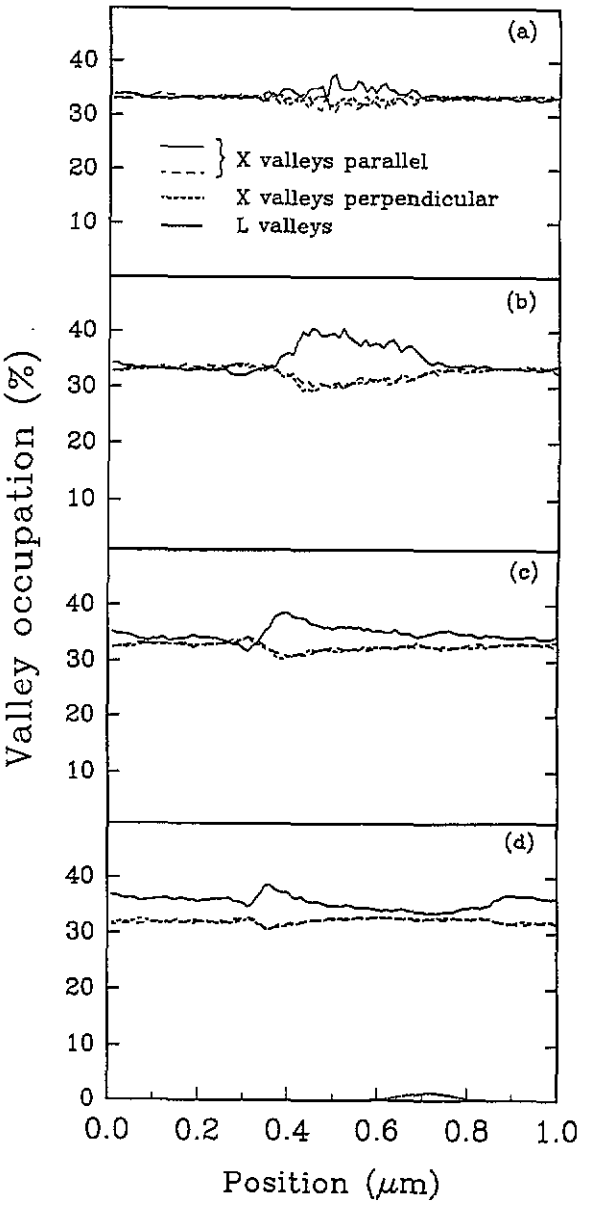

Figure 10. Valley occupation along the n^+nn^+ structure for different biases: 0.1 V (*a*) , 0.6 V (*b*), 2 V (*c*) and 4 V (*d*). The line for the L valleys corresponds to the total valley occupation of the four L valleys.

a submicrometre diode (n^+nn^+) in the ⟨100⟩ and ⟨111⟩ crystallographic directions. In the homogeneous structure several differences between the two directions of the applied voltage appear, which are reflected in the anisotropy present in the current density–voltage characteristic. This effect has been extensively explained through the drift velocity–electric field results on bulk Si. At the same time the simulation of the n^+nn^+ structure has been carried out. In this structure the anisotropy effects are less pronounced due to its inhomogeneity. In any case the differences in current density and saturation are explained in terms of the different occupation of the X valleys depending on the direction of the electric field.

Acknowledgments

This work has been funded through an agreement with

IBM SAE, and SA-14/14/92 project from the Consejería de Cultura de la Junta de Castilla y León.

References

[1] Fischetti M V and Laux S E 1991 *IEEE Trans. Electron Devices* **38** 650

[2] Izuka T and Fukuma M 1990 *Solid-State Electron.* **33** 27

[3] Meinerzhagen B and Engl W L 1988 *IEEE Trans. Electron Devices* **35** 689

[4] Sandborn P A, Rao A and Blakey P A 1989 *IEEE Trans. Electron Devices* **36** 1244

[5] See, for instance, Tang T-W, Ramaswamy S and Nam J 1993 *IEEE Trans. Electron Devices* **40** 1469 and references therein

[6] Jacoboni C and Lugli P 1989 *The Monte Carlo Method for Semiconductor Device Simulation* (Vienna: Springer)

[7] Crandle T L, East J R and Blakey P A 1989 *IEEE Trans. Electron Devices* **36** 300

[8] Fiegna C and Sangiorgi E 1993 *IEEE Trans. Electron Devices* **40** 619

[9] Moglestue C 1986 *IEEE Trans. Computer-Aided Design* **5** 326

[10] Tang J and Hess K 1983 *J. Appl. Phys.* **54** 5139

[11] Fischetti M and Laux S 1988 *Phys. Rev.* B **38** 9721

[12] Sano N and Yoshii A 1992 *Phys. Rev.* B **45** 4171

[13] Kunikiyo T, Takenaka M, Kamakura Y, Yamaji M, Mizuno H, Morifuji M, Taniguchi K and Hamaguchi C 1994 *J. Appl. Phys.* **75** 297

[14] Baranger H U, Pelouard J-L, Pône J-F and Castagné R 1987 *Appl. Phys. Lett.* **51** 1708

[15] Tian H, Kim K W, Littlejohn M A, Mishra U K and Hashemi M 1992 *J. Appl. Phys.* **72** 5695

[16] Zimmermann J and Constant E 1980 *Solid-State Electron.* **23** 915

[17] Nguyen P T, Navon D H and Tang T-W 1985 *IEEE Trans. Electron Devices* **32** 783

[18] Varani L, Kuhn T, Reggiani L and Perlès Y 1993 *Solid-State Electron.* **36** 251

[19] Martín M J, González T, Velázquez J and Pardo D 1993 *Semicond. Sci. Technol.* **8** 1291

[20] González T, Velázquez J, Gutiérrez P and Pardo D 1991 *Semicond. Sci. Technol.* **6** 862

[21] González T, Velázquez J, Guitérrez P and Pardo D 1992 *Semicond. Sci. Technol.* **7** 31

[22] Chelikowsky T and Cohen M 1976 *Phys. Rev.* B **14** 556; see also Cohen M and Chelikowsky J 1988 *Electronic Structure and Optical Properties of Semiconductors* (Berlin: Springer)

[23] Lee C, Logan R, Batdorf, Kleimack J and Wiegmann W 1964 *Phys. Rev.* **134** A761

[24] Van Overstraeten R and De Man H 1970 *Solid-State Electron.* **13** 583

[25] Woods M, Johnson W and Lampert M 1973 *Solid-State Electron.* **16** 381

[26] Takayanagi I, Matsumoto K and Nakamura J 1992 *J. Appl. Phys.* **72** 1989

[27] Jacoboni C and Reggiani L 1983 *Rev. Mod. Phys.* **55** 635

[28] Canali C, Jacoboni C, Nava F, Ottaviani G and Albergiri-Quaranta A 1975 *Phys. Rev.* B **12** 2265

[29] Sano N, Aoki T, Tomizawa M and Yoshii A 1990 *Phys. Rev.* B **41** 12122

[30] Hockney R and Eastwood J 1981 *Computer Simulation Using Particles* (New York: McGraw-Hill)

[31] Shockley W 1950 *Electrons and Holes in Semiconductors* (New York: Van Nostrand)

[32] Press W H, Flannery B P, Teukolsky S A and Vetterling W T 1989 *Numerical Recipes. The Art of Scientific Computing* (New York: Cambridge University Press)